Eur. Phys. J. E **33**, 27–39 (2010)
DOI 10.1140/epje/i2010-10654-7

THE EUROPEAN PHYSICAL JOURNAL E

Regular Article

Hydrodynamic interaction between two trapped swimming model micro-organisms

R. Matas Navarro[a] and I. Pagonabarraga

Departament de Física Fonamental, Universitat de Barcelona, C. Martí i Franqués 1, 08028, Barcelona, Spain

Received 16 April 2010 and Received in final form 30 July 2010
Published online: 23 September 2010 –

Abstract. We present a theoretical study of the behaviour of two active particles under the action of harmonic traps kept at a fixed distance away from each other. We classify the steady configurations the squirmers develop as a function of their self-propelling velocity and the active stresses the swimmers induce around them. We have further analyzed the stability of such configurations, and have found that the ratio between their self-propelling velocity and the apolar flow generated through active stresses determines whether collinear parallel squirmers or perpendicularly swimming particles moving away from each other are stable. Therefore, there is a close connection between the stable configurations and the active mechanisms leading to the particle self-propulsion. The trap potential does not affect the stability of the configurations; it only modifies some of their relevant time scales. We have also observed the development of characteristic frequencies which should be observable. Finally, we show that the development of the hydrodynamic flows induced by the active particles may be relevant even when its time scale orders of magnitude smaller than the other present characteristic time scales and may destabilize the stable configurations.

1 Introduction

Natural and artificial swimmers at small scales, when the fluid inertia is negligible, exploit a wide variety of mechanisms to overcome reciprocal cyclic motion [1]. Natural micro-organisms have developed appendices, such as flagella or cilia, or deform their shape to displace in a suspending fluid [2]. Artificial swimmers sometimes have mimicked the strategies of natural organisms [3–5], while in some other situations microrobots have exploited heterogeneous catalysis or electrochemical reactions [6] or the reaction to actuating fields [7,8] to induce net propulsion of microscale particles. Since viscous transport is dominant, in all previous examples the swimmers generate a net fluid flow which decays algebraically. Such flows lead to dynamic correlations between swimmers if they move in a suspension, affecting swimmer collisions [9] and modifying swimmers collective properties leading to long-range correlations [10], large density fluctuations [11], transient clustering [12] and affect the effective diffusion in swimmer suspensions [13]. At large scales, the basic hydrodynamic features introduce by the internal activity of the swimmers can be captured taking into account the stress induced by these active, suspended constituents [14,15] and the active flows and their stability at long scales have been analyzed [16,17]. The active stress which characterizes the contribution of the swimmers to the fluid can also be captured in swimmer resolved models [18].

[a] e-mail: ricardmn@ffn.ub.es

The use of model swimmers has proved a fruitful approach to understand the physics of swimming at low Reynolds numbers. Models have been sometimes motivated by their biological analogues, such as flagella motion described by Taylor [19,20], but in parallel there has been a pursuit of simple swimmers which clarify the basic mechanisms underlying self-propulsion. For example, the three-sphere swimmer [21] has allowed a systematic and detailed analysis of propulsion at small scales for a pair of swimmers [22].

Lighthill [23] proposed a simple model to study the swimming properties of ciliated micro-organisms. The subsequent development of Blake [24] identifies clearly the connection between the active processes generating a slip velocity on the micro-organism surface and the hydrodynamic flow they induce around them. This approach does not reproduce in detail the swimming of any micro-organism and does not relate the active velocity to the corresponding internal mechanisms, but it offers the possibility to perform a systematic study of their collective hydrodynamics [25,26] and structure formation [27].

We will characterize the hydrodynamic coupling of two such swimmers confined by harmonic traps. We will disregard other interactions among them, such as chemotaxis or quorum sensing, to clarify the relevance of active coupling through the flows they generate. Optical traps have already been used to evaluate the hydrodynamics interaction between a pair of objects such as polymer-coated spheres [28] and also to study the properties of the

self-propulsion of bacteria like the efficiency of *E. coli* [29], the measurement of the rotation of *V. alginolyticus* flagella [30] or even some collective dynamic features [31].

The motion of swimmers against a confining potential leads to configurations where the particles do not move, but generate flow around them. Rather than analyzing the pumping behavior of such type of motion, we will focus on the ability of swimmer pair to reach stable steady configurations, and how do they depend on the intrinsic properties of the swimmers. Such an analysis may be of experimental interest, since it shows that optical traps can help to characterize the intrinsic features of active swimmers. Once the relevant dimensionless parameters and relevant time scales have been identified, we consider the situation where the time scales in which induced flows develop are not necessarily much smaller than other characteristic time scales in the system and have found that this memory effect may change qualitatively in some circumstances the behavior of the squirmer pair, indicating the need to treat the motion of the swimmers and the corresponding flow fields on the same footing.

We will first introduce in detail the squirmer model which will be used subsequently. In sect. 3 we derive the evolution equations of a pair of squirmers confined by harmonic traps and will identify the relevant parameters which will determine the allowed stationary configurations, described in sect. 4. After analysing the configuration stability in sect. 5, we discuss the relevant time scales in the different configurations and their oscillatory behavior. In sect. 6 we introduce a simple model to account for the propagation of the induced active flows and characterize its impact in the stability of the stable pair configurations obtained previously. We conclude with a discussion of the main results obtained and their impact and implications.

2 Squirmer model

The squirmer activity is characterized by an intrinsic director, $\mathbf{e}$, which moves rigidly with the particle. We assume that the internal activity generates an axisymmetric slip velocity at the squirmer's spherical surface

$$\mathbf{u}_s = \sum_{i=1}^{\infty} \frac{2B_n}{n(n+1)} \left[-\mathbf{1} + \frac{\tilde{\mathbf{r}}\tilde{\mathbf{r}}}{\tilde{r}^2} \right] \cdot \mathbf{e} P_n' \left(\mathbf{e} \cdot \frac{\tilde{\mathbf{r}}}{\tilde{r}} \right), \quad (1)$$

where P_n is the n-th Legendre polynomial, $\tilde{\mathbf{r}}$ stands for the position vector with respect to the squirmer's center of mass, and at the particle surface $\tilde{r} = |\tilde{\mathbf{r}}| = a$. The surface velocity $\mathbf{u}_s$ generates a fluid flow with an asymptotic algebraic decay whose exponent is determined by the degree of the corresponding Legendre polynomial. Therefore, the amplitudes, B_n, identify the component of the surface velocity associated with a particular flow feature. We will restrict ourselves to a minimal squirmer characterized by the first two terms in the previous general expansion and consider therefore $B_i = 0$ for $i > 2$. This simplified model captures the polarity associated to the squirmer swimming velocity and the apolar stresses generated by the surface waves [25]. An isolated squirmer moves asymptotically at a constant speed $\mathbf{v}_0 = \frac{2}{3} B_1 \mathbf{e}$ and generates a vorticity field around it proportional to B_2. The sign of this coefficient determines if the squirmer behaves as a puller ($B_2 > 0$) or as a pusher ($B_2 < 0$), also known as contractile or extensile, respectively. Contractile swimmers pull the fluid along the direction of movement and push it along the normal direction. Extensile swimmers, on the contrary, push fluid along the propelling squirmer direction and pull along the perpendicular one. Motile algae, like *Chlamydomonas*, behave as pullers while *Eshcherichia coli* can be regarded as pushers. The relevance of apolar stresses in front of polar self-propulsion in this simplified model is captured by the ratio of the two amplitudes, $\beta = B_2/B_1$ [25], the main ingredient which defines the microswimmer behaviour. The sign of β, through B_2, identifies both the microswimmers according to the forces they exert on the surrounding fluid (pullers or pushers) and quantifies the relevance of self-propulsion; from apolar motion $|\beta| \gg 1$, where active vorticity dominates the flow, to polar swimmers $|\beta| \ll 1$.

The velocity field generated by a squirmer when polarity is determined by B_1 and the active stresses by B_2 reads

$$\mathbf{U}_p(\tilde{\mathbf{r}}, \mathbf{e}) = -\frac{1}{3}\frac{a^3}{\tilde{r}^3} B_1 \mathbf{e} + B_1 \frac{a^3}{\tilde{r}^3} \mathbf{e} \cdot \hat{\tilde{r}} \hat{\tilde{r}} - \frac{a^2}{\tilde{r}^2} B_2 P_2 \left(\mathbf{e} \cdot \hat{\tilde{r}} \right) \hat{\tilde{r}}. \quad (2)$$

We will disregard thermal fluctuations, since microorganisms are usually larger than a few micrometers in size. Since we want to analyze in detail the dynamic coupling between a pair of squirmers, we will disregard tumbling or other mechanisms which allow micro-organisms to change their direction of propagation. This assumption is valid whenever the tumbling frequency becomes smaller than any other relevant time scale in the response of the system. Even if tumbling needs to be taken into account to describe the precise squirmers' trajectories, the understanding gained in its absence will help to clarify the behavior of trapped micro-organisms under general conditions. The stochastic response inherent to tumbling will also be influenced by the configurations squirmers tend to adopt in its absence. Therefore, analyzing only the evolution on the inter-tumbling time scale, assumed much larger than the typical rotational and translational time scales of the particles, constitutes a relevant limit which must be analyzed in detail. Moreover, in some micro-organisms the tumbling frequency can be tuned experimentally controlling the solvent properties, *e.g.* its temperature in *Escherichia coli* [32] or the cation concentration in *Bacilus subtilis* [33].

3 Squirmers in harmonic traps

We will analyze the dynamic behavior of a pair of identical squirmers trapped in two harmonic traps kept a distance d away from each other. A single squirmer confined in a harmonic trap characterized by a stiffness $\tilde{\boldsymbol{\kappa}}$, a diagonal tensor, will generate a fluid flow as a result of the competition between self-propulsion and the trap stiffness which

will differ from the one induced by free swimming, eq. (2). The confining trap force grows linearly as the squirmer, at position $\tilde{\mathbf{r}}_s$, deviates from the minimum of the harmonic trap, $\tilde{\mathbf{r}}_0$, $\mathbf{F}_h = -\tilde{\boldsymbol{\kappa}} \cdot (\tilde{\mathbf{r}}_s - \tilde{\mathbf{r}}_0)$. As it moves, the squirmer generates a fluid flow of magnitude

$$\begin{aligned}\mathbf{U}(\tilde{\mathbf{r}} - \tilde{\mathbf{r}}_s, \mathbf{e}, \tilde{\mathbf{r}}_0) &= \mathbf{U}_p(\tilde{\mathbf{r}} - \tilde{\mathbf{r}}_s, \mathbf{e}) \\ &-\frac{3}{4} a\boldsymbol{\kappa} \cdot \frac{\tilde{\mathbf{r}}_s - \tilde{\mathbf{r}}_0}{|\tilde{\mathbf{r}} - \tilde{\mathbf{r}}_s|} \cdot \left(\mathbf{1} + \frac{(\tilde{\mathbf{r}} - \tilde{\mathbf{r}}_s)(\tilde{\mathbf{r}} - \tilde{\mathbf{r}}_s)}{|\tilde{\mathbf{r}} - \tilde{\mathbf{r}}_s|^2} \right), \end{aligned} \tag{3}$$

where we have introduced the characteristic frequency tensor, $\boldsymbol{\kappa} = \tilde{\boldsymbol{\kappa}}/6\pi\mu a$. In a steady state, the particle behaves as a pump [34]; the squirmer does not move, but generates flow around it. If tumbling can be disregarded, an isolated squirmer will reach a steady position which arises from a balance of self-propulsion and the confining trap force.

We capture the coupling between two squirmers trapped by corresponding harmonic traps a distance $|\tilde{\mathbf{r}}_{0.1} - \tilde{\mathbf{r}}_{0,2}|$ away from each other making use of Faxén equalities [35]. These relations are valid provided the two squirmers are not close to each other, *i.e.* $\frac{a}{\tilde{r}} \ll 1$; a condition one can control by placing the harmonic traps appropriately in space. Within this assumption, the equations of motion for the pair of identical squirmers read

$$\begin{aligned}\frac{\mathrm{d}\tilde{\mathbf{r}}_i}{\mathrm{d}\tilde{t}} &= \tilde{\mathbf{v}}_i, \\ \frac{\mathrm{d}\tilde{\mathbf{v}}_i}{\mathrm{d}\tilde{t}} &= \frac{6\pi\mu a}{m} \left[-\tilde{\mathbf{v}}_i + \frac{2}{3} B_1 \mathbf{e}_i \right. \\ &\quad \left. + \left(1 + \frac{a^2}{6} \tilde{\nabla}^2 \right) \mathbf{U}_j - \kappa(\tilde{\mathbf{r}}_i - \tilde{\mathbf{r}}_{0,i}) \right], \\ \frac{\mathrm{d}\mathbf{e}_i}{\mathrm{d}\tilde{t}} &= \tilde{\boldsymbol{\Omega}}_i \times \mathbf{e}_i, \\ \frac{\mathrm{d}\tilde{\boldsymbol{\Omega}}_i}{\mathrm{d}\tilde{t}} &= \frac{8\pi\mu a^3}{I} \left[-\tilde{\boldsymbol{\Omega}}_i + \frac{1}{2} \tilde{\nabla} \times \mathbf{U}_j \right], \end{aligned} \tag{4}$$

for $i, j = 1, 2$ and $i \neq j$, and where $\mathbf{U}_j \equiv \mathbf{U}(\tilde{\mathbf{r}}_{ij}, \mathbf{e}_j, \tilde{\mathbf{r}}_{0,j})$ is the velocity induced by squirmer j at the position of particle i.

The total drag force with respect to the intrinsic swimmer velocity accounts for the friction induced by the flow generated by the neighbouring particle according to first Faxén law. It assumes that the reference particle moves in the background flow generated by the swimming neighbour when it is isolated. Accordingly, we use the second Faxén law to derive the drag torque, which assumes that the reference particle rotates in the presence of the vorticity flow induced by the neighbouring swimmer when it is isolated.

The vorticity induced by squirmer i at position $\tilde{\mathbf{r}}$ relative to the particle center of mass can be expressed as

$$\frac{1}{2} \tilde{\nabla} \times \mathbf{U}_i = \frac{3}{2} \frac{a^2}{\tilde{r}^5} B_2 (\mathbf{e}_i \cdot \tilde{\mathbf{r}}) \tilde{\mathbf{r}} \times \mathbf{e}_i + \frac{3}{4} \frac{a}{\tilde{r}^2} \boldsymbol{\kappa} \cdot \hat{\mathbf{r}} \times (\tilde{\mathbf{r}}_i - \tilde{\mathbf{r}}_{0,i}). \tag{5}$$

Since we are interested in the main features that activity imparts to the coupling between the pair of swimmers, we will disregard the Laplacian of the induced flow field which features in the previous equations in front of the interaction coming directly from the fluid field itself. The disregarded terms do not affect the main conclusions of the subsequent analysis for $\frac{a}{\tilde{r}} \ll 1$.

It turns out to be convenient to analyze the pair motion in terms of the relative and center of mass variables

$$\begin{aligned}\tilde{\mathbf{r}} &= \tilde{\mathbf{r}}_2 - \tilde{\mathbf{r}}_1, \qquad \tilde{\mathbf{v}} = \tilde{\mathbf{v}}_2 - \tilde{\mathbf{v}}_1, \\ \tilde{\mathbf{r}} &= \frac{1}{2}(\tilde{\mathbf{r}}_2 + \tilde{\mathbf{r}}_1), \qquad \tilde{\mathbf{v}} = \frac{1}{2}(\tilde{\mathbf{v}}_2 + \tilde{\mathbf{v}}_1). \end{aligned} \tag{6}$$

We assume that the confining potential in one direction is much stiffer than in the other two with equal characteristic frequency κ, and consider accordingly the displacement of the squirmers in a plane which coincides with $z = 0$. Hence $\tilde{\mathbf{r}} = \tilde{x}\mathbf{e}_x + \tilde{y}\mathbf{e}_y$, $\tilde{\mathbf{R}} = \tilde{X}\mathbf{e}_x + \tilde{Y}\mathbf{e}_y$ and we will use the traps' positions to define the orientation of the coordinate axis. Accordingly, $\tilde{\boldsymbol{\Omega}}_i = \tilde{\Omega}_i \mathbf{e}_z$ and we take the pair center of mass position associated to the minima of the harmonic traps, $\tilde{\mathbf{R}}^0 = (\tilde{\mathbf{r}}_{0,1} + \tilde{\mathbf{r}}_{0,2})/2 = 0$ as the coordinate origin. The direction characterizing the relative position of the two traps is taken along the y-axis, $\tilde{\mathbf{r}}_0 \equiv \tilde{\mathbf{r}}_{0,1} - \tilde{\mathbf{r}}_{0,2} = d\mathbf{e}_y$.

To analyze the motion and configurations of the squirmer, we introduce $v_0 = B_1 + \delta^2 B_2$ as a characteristic speed which includes the squirmer self-propulsion as well as the perturbation induced by the neighboring particle, where $\delta \equiv \frac{a}{d}$ corresponds to the inverse of the scaled distance d between the harmonic traps. If we further express distances in units of d and times in units of $\frac{d}{v_0}$, we can rewrite the previous equations of motion in dimensionless units as

$$\begin{aligned}\frac{\mathrm{d}\mathbf{e}_i}{\mathrm{d}t'} &= -\omega_i' \mathbf{e}_z \times \mathbf{e}_i, \\ \frac{\mathrm{d}\omega_i'}{\mathrm{d}t} &= -\frac{15}{Re\,\delta} \left[\omega_i' + \kappa d \frac{b_2}{v_0} \frac{\mathbf{e}_j \cdot \mathbf{r}(\mathbf{e}_j \times \mathbf{r}) \cdot \mathbf{e}_z}{r^5} \right. \\ &\quad \left. + \frac{3}{4} \delta \frac{\kappa d}{v_0} \left(\mathbf{r} \times \frac{\mathbf{R} - \frac{\mathbf{r}_0}{2}}{r^3} \right) \cdot \mathbf{e}_z \right], \\ \frac{\mathrm{d}\mathbf{r}}{\mathrm{d}t} &= \mathbf{v}', \qquad \frac{\mathrm{d}\mathbf{R}}{\mathrm{d}t} = \mathbf{V}', \\ \frac{\mathrm{d}\mathbf{v}'}{\mathrm{d}t} &= \frac{9}{2} \frac{1}{Re\,\delta} \left[-\mathbf{v}' + \kappa d \frac{b_1}{v_0} (\mathbf{e}_2 - \mathbf{e}_1) \left(1 + \frac{1}{2} \frac{\delta^3}{r^3} \right) \right. \\ &\quad - \frac{3}{2} \kappa d \delta^3 \frac{b_1}{v_0} \frac{(\mathbf{e}_2 - \mathbf{e}_1) \cdot \mathbf{r}}{r^5} \mathbf{r} - \frac{2}{3} \kappa d \frac{b_2}{v_0} (P_{22} + P_{21}) \frac{\mathbf{r}}{r^3} \\ &\quad \left. - \frac{\kappa d}{v_0} (\mathbf{r} - \mathbf{r}^0) \left(1 - \frac{3}{4} \frac{\delta}{r} \right) + \frac{3}{4} \delta \frac{\kappa d}{v_0} \frac{\mathbf{r} - \mathbf{r}^0}{r^3} \cdot \mathbf{r}\mathbf{r} \right], \\ \frac{\mathrm{d}\mathbf{V}'}{\mathrm{d}t} &= \frac{9}{2} \frac{1}{Re\,\delta} \left[-\mathbf{V}' + \frac{1}{2} \kappa d \frac{b_1}{v_0} (\mathbf{e}_2 + \mathbf{e}_1) \left(1 - \frac{1}{2} \frac{\delta^3}{r^3} \right) \right. \\ &\quad + \frac{3}{4} \kappa d \delta^3 \frac{b_1}{v_0} \frac{(\mathbf{e}_2 + \mathbf{e}_1) \cdot \mathbf{r}}{r^5} \mathbf{r} + \frac{2}{3} \kappa d \frac{b_2}{v_0} \frac{P_{22} - P_{21}}{2} \frac{\mathbf{r}}{r^3} \\ &\quad \left. - \frac{\kappa d}{v_0} (\mathbf{R} - \mathbf{R}^0) \left(1 + \frac{3}{4} \frac{\delta}{r} \right) - \frac{3}{4} \delta \frac{\kappa d}{v_0} \frac{\mathbf{R} - \mathbf{R}^0}{r^3} \cdot \mathbf{r}\mathbf{r} \right], \end{aligned} \tag{7}$$

where $P_{2i} = \frac{1}{2}(3(\mathbf{e}_i \cdot \mathbf{r}/r)^2 - 1)$ and $Re \equiv \frac{a v_0}{\nu}$ corresponds to the squirmer's Reynolds number. The previous equations show that the behavior of the squirmer pair under

the action of traps is characterized by the parameters

$$b_1 = \frac{2}{3}\frac{B_1}{d\kappa}\,, \qquad b_2 = \frac{3}{2}\frac{\delta^2 B_2}{d\kappa}\,,$$

which are the ratio of the velocity induced by the self-polar and neighbour apolar activity to the characteristic velocity associated to the harmonic trap, respectively.

We will consider squirmers which move at low Re numbers, as is the case in micro-organisms, where sizes are of the order of micrometers and velocities are not larger than a few hundred micrometers per second. For example, for opalina $100\,\mu$m in size moving in water at a speed $500\,\mu$m/s, $Re \sim 0.005$. We will accordingly disregard inertia and consider the limit $Re \to 0$ in eqs. (7). It is then useful to introduce the rescaled time $t = t' d\kappa/v_0$, which affects all angular and linear velocities (*e.g.*, $\Omega_i = \Omega_i' v_0/\kappa d$), and to consider the motion along the radial and tangential components of the pair. To this end, we define radial and in-plane tangential components of a general vector $\mathbf{A}$ as

$$A^r = \hat{r}\cdot\mathbf{A}, \qquad A^t = (\hat{r}\times\mathbf{A})\cdot\hat{z} \tag{8}$$

and introduce the projections $\mathbf{e}_i\cdot\hat{r} = \cos\theta_i$ and $\mathbf{r}_0\cdot\hat{r} = r_0\cos\Psi$. Equations (7) reduce then to

$$\begin{aligned}
&\frac{\mathrm{d}\theta_i}{\mathrm{d}t} = \Omega_i - \frac{v^t}{r}\,, \quad i=1,2,\\
&\frac{\mathrm{d}r}{\mathrm{d}t} = v^r, \qquad \frac{\mathrm{d}\Psi}{\mathrm{d}t} = \frac{v^t}{r}\,,\\
&\frac{\mathrm{d}R^r}{\mathrm{d}t} = V^r + \frac{v^t R^t}{r}\,, \qquad \frac{\mathrm{d}R^t}{\mathrm{d}t} = V^t - \frac{v^t R^r}{r}\,,
\end{aligned} \tag{9}$$

where the relevant velocity components read

$$\begin{aligned}
\Omega_1 &= b_2\frac{\cos\theta_2\sin\theta_2}{r^3} - \frac{3}{4}\delta\frac{R^t - \frac{\cos\Psi}{2}}{r^2}\,,\\
\Omega_2 &= b_2\frac{\cos\theta_1\sin\theta_1}{r^3} + \frac{3}{4}\delta\frac{R^t + \frac{\cos\Psi}{2}}{r^2}\,,\\
v^r &= b_1(\cos\theta_2 - \cos\theta_1) - \frac{2}{3}b_2\frac{P_2^2 + P_2^1}{r^2}\\
&\quad -(r-\sin\Psi)\left(1 - \frac{3}{2}\frac{\delta}{r}\right),\\
v^t &= b_1(\sin\theta_2 - \sin\theta_1) + \cos\Psi\left(1 - \frac{3}{4}\frac{\delta}{r}\right),\\
V^r &= \frac{1}{2}b_1(\cos\theta_2 + \cos\theta_1) + \frac{1}{3}b_2\frac{P_2^2 - P_2^1}{r^2} - R^r\left(1 + \frac{3}{2}\frac{\delta}{r}\right),\\
V^t &= \frac{1}{2}b_1(\sin\theta_2 + \sin\theta_1) - R^t\left(1 + \frac{3}{4}\frac{\delta}{r}\right).
\end{aligned} \tag{10}$$

For simplicity, we neglected terms of order δ^3 arising as subdominant contributions from powers of the squirmers separation, $1+\delta^3$.

4 Stationary arrangements of a pair of trapped squirmers

In order to characterize the motion of the squirmer pair confined by the harmonic traps at a prescribed distance, we start by analyzing the stationary configurations, which we derive from eqs. (7),

$$b_2\frac{\mathbf{e}_2\cdot\mathbf{r}\,\mathbf{r}\times\mathbf{e}_2}{r^2} - \frac{3\delta}{4}\mathbf{r}\times\left(\mathbf{R} - \frac{\mathbf{r}^0}{2}\right) = 0, \tag{11}$$

$$b_2\frac{\mathbf{e}_1\cdot\mathbf{r}\,\mathbf{r}\times\mathbf{e}_1}{r^2} + \frac{3\delta}{4}\mathbf{r}\times\left(\mathbf{R} + \frac{\mathbf{r}^0}{2}\right) = 0, \tag{12}$$

$$\begin{aligned}
&b_1(\mathbf{e}_2 - \mathbf{e}_1) - \frac{3\delta^3}{2}b_1\frac{(\mathbf{e}_2 - \mathbf{e}_1)\cdot\mathbf{r}}{r^5}\mathbf{r} - \frac{2}{3}b_2(P_2^2 + P_2^1)\frac{\mathbf{r}}{r^3}\\
&\quad -(\mathbf{r} - \mathbf{r}^0)\left(1 - \frac{3}{4}\frac{\delta}{r}\right) + \frac{3\delta}{4}\frac{\mathbf{r} - \mathbf{r}^0}{r^3}\cdot\mathbf{r}\mathbf{r} = 0,
\end{aligned} \tag{13}$$

$$\begin{aligned}
&b_1(\mathbf{e}_2 + \mathbf{e}_1) + \frac{3\delta^3}{2}b_1\frac{(\mathbf{e}_2 + \mathbf{e}_1)\cdot\mathbf{r}}{r^5}\mathbf{r} + \frac{2}{3}b_2(P_2^2 - P_2^1)\frac{\mathbf{r}}{r^3}\\
&\quad -2(\mathbf{R} - \mathbf{R}^0)\left(1 + \frac{3}{4}\frac{\delta}{r}\right) - \frac{3\delta}{2}\frac{\mathbf{R} - \mathbf{R}^0}{r^3}\cdot\mathbf{r}\mathbf{r} = 0.
\end{aligned} \tag{14}$$

Making use of the fact that the self-propelling directors are unit vectors $\mathbf{e}_i\cdot\mathbf{e}_i = 1$, the previous equations determine all the relevant variables characterizing the squirmer pair. After some algebra involving these four equations, eqs. (11) and (12) can be restated as

$$\begin{aligned}
\mathbf{r}\cdot\mathbf{e}_1\,\mathbf{r}\times\mathbf{e}_1 &= -\frac{3\delta}{4}\frac{b_1}{b_2}\frac{r^2}{1 - \left(\frac{3}{4}\frac{\delta}{r}\right)^2}\left[\mathbf{r}\times\mathbf{e}_1 - \frac{3}{2}\frac{\delta}{r}\mathbf{r}\times\mathbf{e}_2\right],\\
\mathbf{r}\cdot\mathbf{e}_2\,\mathbf{r}\times\mathbf{e}_2 &= \frac{3\delta}{4}\frac{b_1}{b_2}\frac{r^2}{1 - \left(\frac{3}{4}\frac{\delta}{r}\right)^2}\left[\mathbf{r}\times\mathbf{e}_2 - \frac{3}{2}\frac{\delta}{r}\mathbf{r}\times\mathbf{e}_1\right],
\end{aligned} \tag{15}$$

which, to lowest order in δ read

$$\begin{aligned}
\mathbf{r}\cdot\mathbf{e}_1\,\mathbf{r}\times\mathbf{e}_1 &= -\alpha\left(\mathbf{r}\times\mathbf{e}_1 - \frac{3}{2}\frac{\delta}{r}\mathbf{r}\times\mathbf{e}_2\right),\\
\mathbf{r}\cdot\mathbf{e}_2\,\mathbf{r}\times\mathbf{e}_2 &= \alpha\left(\mathbf{r}\times\mathbf{e}_2 - \frac{3}{2}\frac{\delta}{r}\mathbf{r}\times\mathbf{e}_1\right),
\end{aligned} \tag{16}$$

in terms of the rescaled activity parameter

$$\alpha = \frac{3}{4}\frac{b_1\delta}{b_2}r.$$

This parameter represents the ratio between the self-propulsion and vorticity amplitudes associated with the squirmers' activity and which characterize their dynamic coupling. Such a coupling becomes explicit if we express the ratio as $\alpha = \frac{r}{2\delta^2}\frac{B_1}{B_2} = \frac{r}{2\delta^2\beta}$, where we can identify the self-propulsion velocity, which provides the polarity strength, and stresslet flow with amplitude $\delta^2 B_2$, the apolar strength. The dependence on δ accounts for the fact that the dynamic coupling decreases with the pair distance.

Consistent with the Faxén approximation, in the subsequent analytical analysis we will assume that neither self-propulsion nor the neighbour influence induce large displacements along the radial direction, and hence $r = 1 + \Delta r$ with $|\Delta r| \ll 1$, and $r \gg \delta$ is always fulfilled.

The steady-state configurations the squirmers can adopt are easily obtained for purely apolar squirmers, for

Table 1. Steady-state orientations for a pair of apolar squirmers, $\alpha = 0$, in terms of the angles (θ_1, θ_2) with respect to the direction which joins the squirmers centers. Due to inherent symmetries, only 7 of the above configurations are physically independent. We have identified these independent configurations with numbers inside each group: {A.1, A.2, A.3}, {B.1, B.2} and {C.1, C.2}, while the lower case letters describe all the symmetrically equivalent configurations.

A	A.1a	$(0,0)$	A.2 $(\pi,0)$	A.3 $(0,\pi)$
	A.1b	(π,π)		
B	B.1a	$(\pi/2,\pi/2)$	B.2a	$(\pi/2,-\pi/2)$
	B.1b	$(-\pi/2,-\pi/2)$	B.2b	$(-\pi/2,\pi/2)$
C	C.1a	$(0,\pi/2)$	C.2a	$(\pi,\pi/2)$
	C.1b	$(0,-\pi/2)$	C.2b	$(\pi,-\pi/2)$
	C.1c	$(\pi/2,\pi)$	C.2c	$(\pi/2,0)$
	C.1d	$(-\pi/2,\pi)$	C.2d	$(-\pi/2,0)$

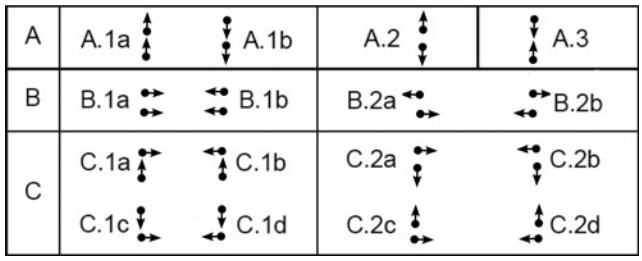

Fig. 1. Orientations of apolar swimmers, $\alpha = 0$, corresponding to the steady-state configurations shown in table 1. Only the relative orientations are relevant, since the possible squirmer displacements are not displayed.

which $\alpha = 0$. In this case swimming is essentially collective since a squirmer cannot move on its own. There exist three families of allowed configurations,

A) *Collinear squimers*, where the pair swims along the same direction, which coincides with the direction of the relative position vector; $\mathbf{r}$, $(\mathbf{r} \times \mathbf{e}_1 = 0, \mathbf{r} \times \mathbf{e}_2 = 0)$.

B) *Parallel squirmers*, where the pair swims along the same direction, which is perpendicular to the direction of their relative position vector; $(\mathbf{r} \cdot \mathbf{e}_1 = 0, \mathbf{r} \cdot \mathbf{e}_2 = 0)$.

C) *Perpendicular squirmers*, where the pair swims along perpendicular directions and one of them is parallel to the direction of their relative position vector; $(\mathbf{r} \cdot \mathbf{e}_i = 0, \mathbf{r} \times \mathbf{e}_j = 0)$, $(i, j = 1, 2)$.

Table 1 lists the 16 steady configurations in terms of the angles introduced in eq. (9). Figure 1 shows the relative orientations for the configurations of table 1 for apolar squirmers, $\alpha = 0$.

We have solved numerically eqs. (15) to characterize the steady-state configurations in terms of the separation between the two particles, r and the relative orientation of the self-propelling squirmers directions, θ_1 and θ_2, as a function of the relevant parameters, b_1 and b_2, and the trap separation, δ.

In order to exploit the simplified steady-state configurations of apolar squirmers it is useful to characterize the

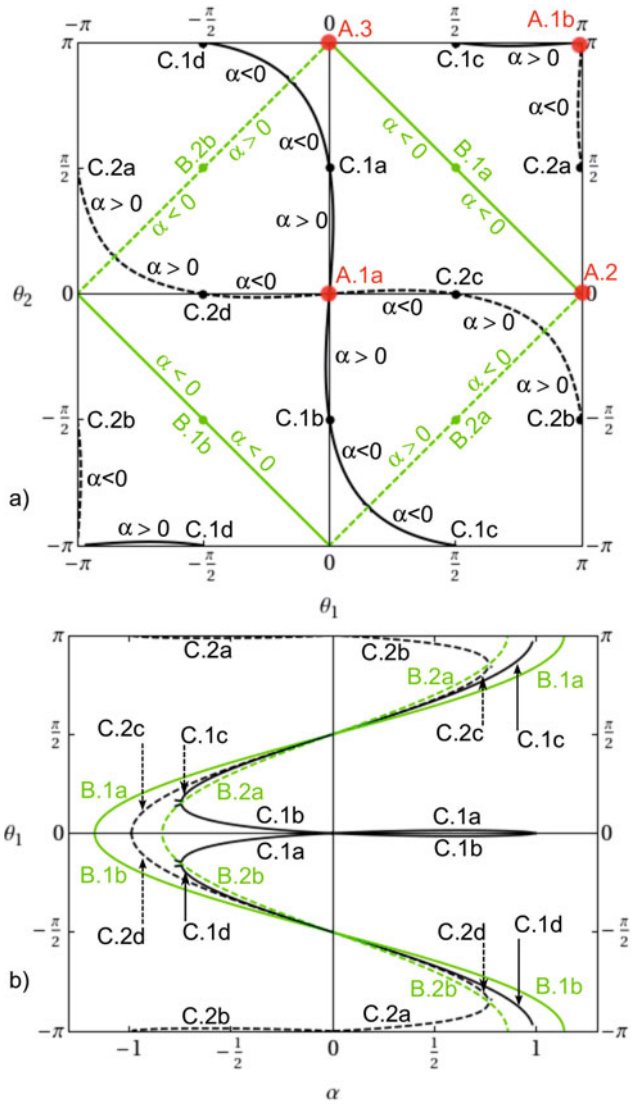

Fig. 2. (Colour online) Steady orientations of a pair of identical squirmers with dimensionless stresslet, $b_2 = 1/200$, moving on two traps a distance $\delta = 1/5$ away from each other. a) Orientations of the two squirmers (θ_1, θ_2) for the different relevant configurations listed in table 1. Red circles correspond to type A, green lines to type B and black lines to type C (big solid circles, light-gray lines and black lines instead if printed without color) configurations. b) Orientation of one squirmer as a function of α for the different relevant configurations displayed in a). Type-A solutions describe straight lines laying over the axes and exist for any α.

squirmers self-propelling features in terms of b_2 and α. In fig. 2(a) we show the orientations of a squirmer pair at a given b_2 and δ on changing the relative apolar strength, α. The sixteen dots characterize the solutions of purely apolar particles, $\alpha = 0$. Starting from one of such configurations, the curves which go through them quantify the orientation change of the pair as α changes. Collinear squirmers (type A) are peculiar, because their orientation does not change with α; only their distance relative to the harmonic trap minima is affected. As a result, big circles

(red in online version) corresponding to an A configuration at $\alpha = 0$, represent also the orientation of the pair at any other value of the squirmer polarity, α. In fig. 2(b), where we show the orientation of one of the two squirmers as a function of the relative polar strength, α, these steady solutions correspond to straight lines degenerated with the horizontal axis.

Parallel squirmers, (B), can swim in the same or opposite directions. The propelling strength modifies their orientation according to

$$\begin{aligned} &\sin\theta_1 = \sin\theta_2, \\ &\cos\theta_1 = -\cos\theta_2 = \alpha\left(1 - \frac{3}{2}\frac{\delta}{r}\right), \end{aligned} \quad \text{(type B.1)}$$

$$\begin{aligned} &\sin\theta_1 = -\sin\theta_2, \\ &\cos\theta_1 = -\cos\theta_2 = \alpha\left(1 + \frac{3}{2}\frac{\delta}{r}\right), \end{aligned} \quad \text{(type B.2)} \qquad (17)$$

which reduce to straight lines when α changes at a fixed distance δ, marked as continuous or dashed lines in fig. 2(a) depending on whether they correspond to parallel or antiparallel swimmers, respectively. As can be appreciated in fig. 2(b), steady configurations of parallel squirmers can develop for α smaller in magnitude than $1/|\alpha_c| = 1 - \frac{3}{2}\frac{\delta}{r}$ and $1/|\alpha_c| = 1 + \frac{3}{2}\frac{\delta}{r}$ for type B.1 (parallel squirmers) and B.2 (antiparallel squirmers), respectively. Hence, irrespectively of the contractile or extensile character of the squirmer, polarity will always eventually disrupt these steady configurations.

Finally, for apolar squirmers which move along perpendicular directions (type C), we can also distinguish two subclasses depending whether their swimming directions tend to approach them (converging configurations (C.1), depicted as solid curves in fig. 2) or tend to move the pair away (diverging configurations (C.2), depicted as dotted curves in fig. 2). Each C.1 configuration becomes a C.2 steady state upon inverting the sign of α and permuting the squirmer index, and viceversa; *i.e.* there is a symmetry in the configuration between extensile and contractile swimmers for this family of steady solutions (*e.g.* configuration C1.d turns to C2.c). Figure 2(b) shows that the behavior for a given configuration type, however, is not symmetric if we move from extensile to contractile squirmers. In all cases, polarity eventually disrupts these steady configurations, as was the case with parallel squirmers. The critical α is of magnitude close to 1, as we can also deduce from the approximated expressions for the steady values of the angles, reported in the appendix.

Although we have concentrated the discussion on the evolution of the steady states in fig. 2 for a particular choice of the trap separation δ and the squirmer active apolar stress b_2, analogous results are obtained upon changing them (data not shown). We have restricted ourselves to parameter ranges where the deviations in the squirmer distance are not large, consistent with the Faxén relations used to derive the equations of motion.

In fig. 3 we display the spatial displacements of the squirmer pair for the same parameters used in fig. 2. For

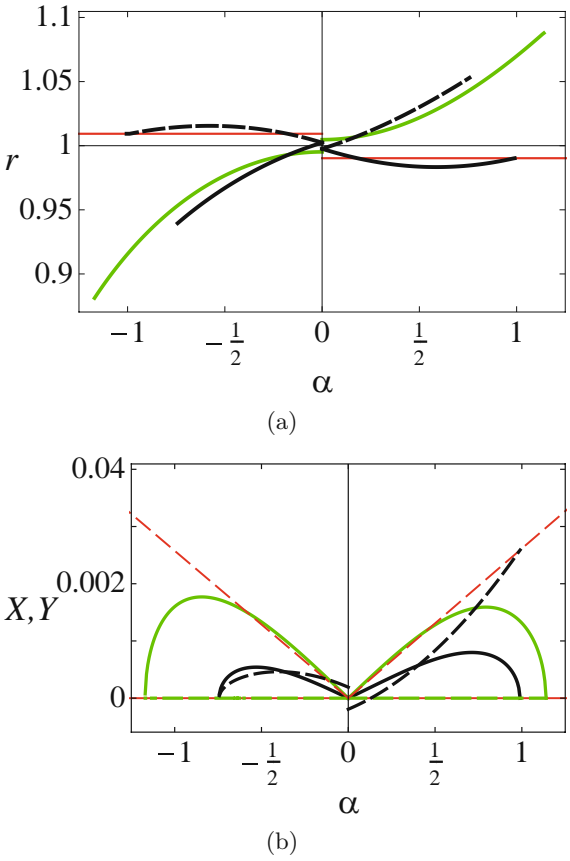

Fig. 3. (Colour online) (a) Distance between the two squirmers for the steady configurations A.1a (red or thin dark gray line), B.1a (green or light gray), C.1a (solid black) and C.2c (dashed black). (b) Position of the center of mass for the steady states A.1a, B.1a and C.1a, using the same style as in (a) but now the solid lines correspond to the X component and the dashed lines depict the Y component, in the reference system where this position is zero when both particles are in the respective trap centers. The parameters used are the ones in fig. 2.

the three families of configurations, the changes in the relative displacement, shown in fig. 3(a), and the deviation of the pair center of mass with respect to the origin, fig. 3(b), are small, with $|\Delta r| \leq 0.1$. Collinear squirmers (class A) display no sensitivity to the magnitude of polarity; only the extensile or contractile character of the active stresses modify slightly the relative separation of the pair as expected. Parallel squirmers (class B) experience an effective repulsion or attraction, while perpendicular squirmers (class C) approach or repel depending on their relative orientation. In all situations a jump in the value of the relative displacement is observed in fig. 3(a) when moving from contractile to extensile squirmers. The amplitude of this jump depends on the magnitude of b_2, which is not zero for purely apolar squirmers at $\alpha = 0$.

Increasing the polarity leads to larger attraction or repulsion between the squirmers, which is further magnified increasing b_2 (data not shown). Eventually the displacements approach the two particles to distances where the equations of motion do not hold any longer. For small

values of the relevant parameters, it is possible to obtain analytic expressions for the steady states for the different arrangements discussed in this section. Even if approximate, such analytic expressions, which are discussed in the appendix, will turn out to be useful to gain insight into the stability of these states, as we will discuss in the next section.

5 Stable configurations of a pair of trapped squirmers

Once we have identified the stationary arrangements for trapped squirmer pairs, we will analyze their stability. To this end, we will consider the linear stability of the steady configurations, which we identify generically as $(\bar{\theta}_1, \bar{\theta}_2, \bar{r}, \bar{\Psi}, \bar{R}^r, \bar{R}^t)$ in terms of the variables introduced in eq. (9). Consistent with the linear stability analysis, the parameter α in this section is taken at the reference squirmer separation, $\bar{r}$. We introduce the small perturbations

$$\begin{aligned} \theta_i &= \bar{\theta}_i + \Delta\theta_i, \quad i = 1, 2, \\ r &= \bar{r} + \Delta r, \qquad \Psi = \bar{\Psi} + \Delta\Psi, \\ R^r &= \bar{R}^r + \Delta R^r, \qquad R^t = \bar{R}^t + \Delta R^t \end{aligned} \tag{18}$$

and linearize the evolution equations around the corresponding steady configurations. The six eigenvalues, $\{\lambda_i\}$ $(i = 1, \ldots, 6)$, provide the rates at which such perturbations will decay back to the steady state or will move away from them. Hence, $\mathrm{Re}(\lambda_i) < 0$ for all six eigenvalues to ensure the linear stability of the corresponding steady state, while a nonzero $|\,\mathrm{Im}(\lambda_i)|$ indicates the existence of a characteristic frequency associated with displacements around the corresponding steady state.

In order to gain insight into the generic features of the eigenvalues, we will consider all the relevant parameters small in magnitude. Then, the steady states discussed in the appendix can be used as a reference and we can expand the eigenvalues in powers of the scaled apolar parameter b_2 (as we will be dealing with $\alpha \sim \mathcal{O}(1)$, small b_2 guarantees small b_1),

$$\lambda_i = \lambda_{i,0} + \lambda_{i,1}(b_2) + \lambda_{i,2}(b_2^2) + \mathcal{O}(b_2^3). \tag{19}$$

We find that for all the steady states there are four eigenvalues with negative contribution to leading order, $\lambda_{i,0} \sim -1$ $(i = 1, \ldots, 4)$, corresponding to four fast decreasing modes, and two eigenvalues with null zeroth-order contribution. Since for small b_1 and b_2 the squirmer separation satisfies $\bar{r} = 1 + \mathcal{O}(b_1, b_2)$, the zeroth-order contributions for the four fast-decreasing modes, neglecting also corrections of order δ^2, are

$$\lambda_{1(2),0} = -1 \pm \frac{3}{4}\delta, \qquad \lambda_{3(4),0} = -1 \pm \frac{3}{2}\delta. \tag{20}$$

In dimensional units these decaying modes evolve on the confining trap time scale, $\tau_0 \sim 1/\kappa$. The remaining two slower modes will control the steady-state stability. These two modes scale with the characteristic times associated to the squirmers' active features, namely $\tau_1 \sim d/B_1$ and $\tau_2 \sim d/|B_2|\delta^2$. An optical trap of stiffness $\tilde{\kappa} \sim 10\,\mathrm{pN}/\mu\mathrm{m}$ [36, 37], leading to a relaxation time of order $\tau_0 \sim 10^{-1}\,\mathrm{s}$ for an organism of size $a \sim 10^2\,\mu\mathrm{m}$, corresponding for example to opalina. If we consider a typical swimming speed of order $10^2\,\mu\mathrm{m/s}$, τ_1 and τ_2 are of order 10 s for a trap separation one order of magnitude larger than the microorganism size. Hence, $\tau_0 \ll \tau_1, \tau_2$; in fact since $\tau_0/\tau_1 \sim b_1$ and $\tau_0/\tau_1 \sim |b_2|$, for micro-organisms it is not difficult to reach the regime $b_1, b_2 < 1$, as assumed earlier. For smaller micro-organisms the hierarchy of times is preserved, although all times diminish; for example, for $a \sim 10\,\mu\mathrm{m}$ all time scales are reduced by one order of magnitude. The numerical analysis of the eigenvalues, without the previous small parameter assumption, validates this scenario as generic even if the separation of time scales previously assumed does not hold, provided that the displacements in the trap do not invalidate the basic assumptions underlying the dynamic model. We have analyzed systematically the stability of the fixed points described in fig. 2 by varying α at fixed δ and $|b_2|$. The results discussed do not change qualitatively upon modifying these two parameters in the range where the Faxén approximation holds.

Figure 4(a) displays the stability of all the fixed points, where the stable configurations are represented with a solid line and the unstable ones with a dashed line. Parallel configurations (type B) are always unstable. The stability of perpendicular squirmers (type C) does not share the symmetry of approaching and diverging stable configurations on changing from extensile to contractile squirmers. As shown in fig. 4(b), while approaching squirmers (type C.1) are unstable for extensile squirmers ($\alpha < 0$) and stable beyond a critical contractile strength, α_t (a regime difficult to appreciate in the figure), diverging ones (type C.2) benefit from the confinement induced by the traps and are always stable. Finally, for $|\alpha| < 1$ collinear squirmers (type A) are always unstable, as depicted in fig. 4(c) and stable otherwise, provided they swim in the same direction (type A.1). For squirmers moving in opposite diverging directions (type A.2), collinear configurations exhibit a small stability window for $|\alpha| \sim 1$, while for approaching directions (type A.3) the steady state is always unstable.

The overall picture described shows that for high polarity, when the self-propelling character of the squirmers dominates, only collinear (type A) stable steady states exist and squirmers tend to swim in the same direction. In the apolar regime, when the active stresses generated by the squirmers dominate, only perpendicularly moving squirmers constitute stable configurations.

To clarify the relevant time scales associated to the stability of the relevant stationary configurations, we will analyze the regime in which b_1 and b_2 are small, when we can benefit from the explicit results for the steady states (as described in the appendix) and the expansion of the eigenvalues introduced in eq. (19).

For collinear parallel swimming (type A.1) the two eigenvalues with $\lambda_{i,0} = 0$, $(i = 5, 6)$ have first- and

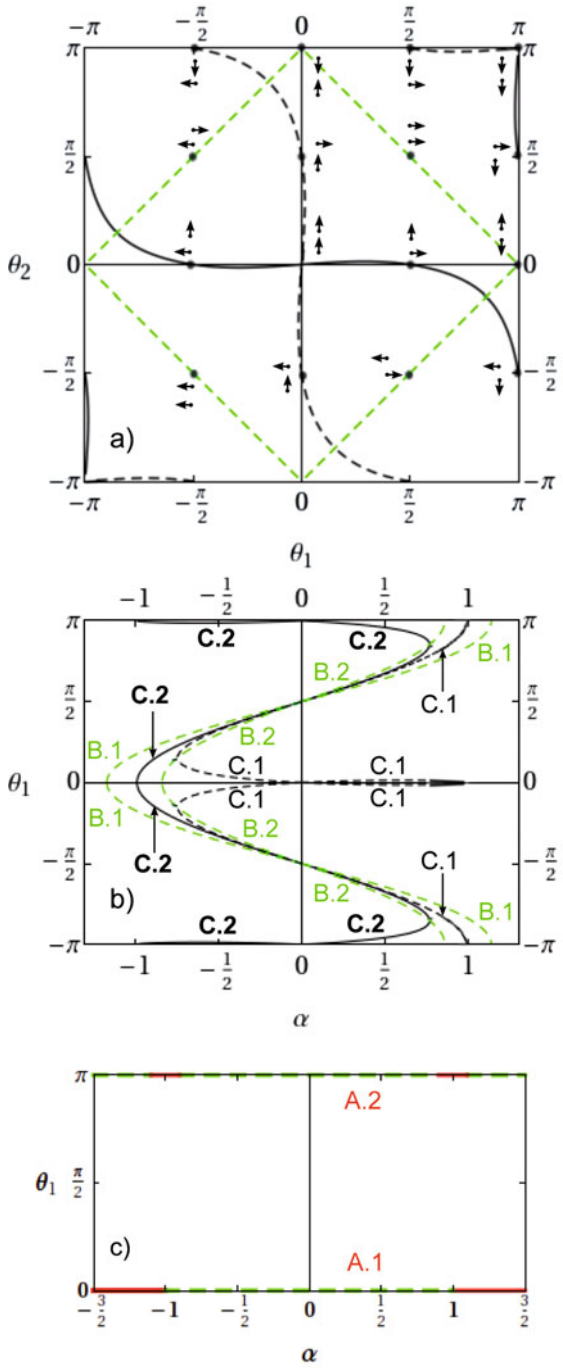

Fig. 4. (Colour online) Stability of the steady configurations of fig. 2. Stable configurations are shown through continuous lines, while unstable arrangements are depicted as dashed curves. Colours and parameters correspond to those introduced in fig. 2. a) Relative orientations of the two squirmers. The small vectors represent the steady orientations of a pair of apolar squirmers ($\alpha = 0$), corresponding to the configurations listed in table 1. b) Orientation of one squirmer as a function of α. c) Stability of collinear A.1 and collinear diverging A.2 steady configurations. Red solid lines denote stable configurations while green (light gray) dashed lines correspond to unstable arrangements. Collinear converging configurations, (A.3), are always unstable and are not depicted.

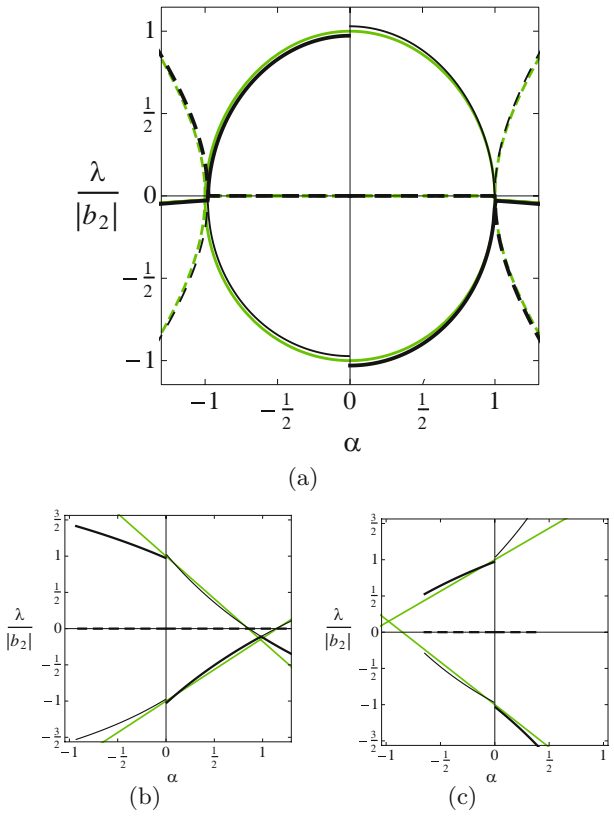

Fig. 5. (Colour online) Eigenvalues, λ_5 (black thin line) and λ_6 (black thick line), which determine the stability of collinear squirmers as a function of the relative apolar strength, α, for the same parameters introduced in fig. 2. The real par of the eigenvalues is shown as solid lines, and the imaginary components as dashed curves. The corresponding analytic predictions are displayed in lighter (green) colour. a) Collinear squirmers, (A.1). b) Collinear diverging configurations (A.2). c) Collinear converging configurations (A.3). In both the latter cases the eigenvalues do not have imaginary components.

second-order components

$$\lambda_{5(6),1} = \pm b_2\sqrt{1-\alpha^2}\,,$$
$$\lambda_{5(6),2} = -\frac{3}{4}b_1^2\delta\left(1-\frac{3}{4}\delta\right), \qquad (21)$$

which agree quantitatively with the numerical results, as depicted in fig. 5(a). It shows that for $|\alpha| < 1$ there is always one eigenvalue with a positive real part. The actual value of the critical α at which the stability changes its character is of order one, but depends on b_1 and b_2 through second-order contributions. The change in stability arises because at large polarity the propulsion in the swimming direction damps perturbations, while for apolar controlled behavior the rotation induced by the active stresses is not opposed by a strong enough drive to keep the prescribed direction. In the unstable regime the steady state will move away on a time scale determined by the active stress, hence of order τ_2, both for contractile and extensile squirmers. In the stable regime, this stress determines the characteristic frequency at which the squirmers

will oscillate around the fixed point; polarity always has a stabilizing effect. The time scale associated to this stabilization mechanism is slower, since it is of second order in b_1. Even if the trap strength cannot modify the stability, it can slow down the stable mode dynamics.

Collinear antiparallel swimming is unstable except for diverging orientations (type A.2) in a small range of $\alpha \sim 1$, as shown in fig. 5(b). The stability is determined again by the first-order contributions of the two eigenvalues which vanish at the lowest order,

$$\lambda_{5(6),1} = \pm b_2 \left(1 - \frac{\alpha}{1 \mp \frac{3}{4}\delta}\right) \quad \text{(type A.2)},$$
$$\lambda_{5(6),1} = \pm b_2 \left(1 + \frac{\alpha}{1 \pm \frac{3}{4}\delta}\right) \quad \text{(type A.3)}. \tag{22}$$

These expressions, in agreement with numerical results as shown in figs. 5(b) and (c) show that destabilization is controlled by the active stress. Accordingly, it takes place on times of order τ_2 although they can be affected by the polarity strength, either accelerating or slowing down the squirmer motion.

For parallel squirmers (type B) there is always one eigenvalue with a positive real part which is prescribed by the active apolar strength and hence evolves on scales of order, τ_2, for parallel (type B.1),

$$\lambda_{5,1} = b_2 \left(1 - \frac{2}{9}\alpha^2 \frac{7 - \frac{27}{2}\delta}{1 + \frac{3}{4}\delta}\right),$$
$$\lambda_{6,1} = -b_2 \left(1 - \frac{2}{9}\alpha^2 \frac{7 - \frac{39}{2}\delta}{1 - \frac{3}{4}\delta}\right), \tag{23}$$

and antiparallel (type B.2),

$$\lambda_{5,1} = b_2 \left(1 - \frac{2}{9}\alpha^2 \frac{7 + \frac{39}{2}\delta}{1 + \frac{3}{4}\delta}\right),$$
$$\lambda_{6,1} = -b_2 \left(1 - \frac{2}{9}\alpha^2 \frac{7 + \frac{27}{2}\delta}{1 - \frac{3}{4}\delta/2}\right), \tag{24}$$

orientations of the squirmers. The numerical results, shown in fig. 6, confirm these theoretical predictions. However, deviations are now larger because in some cases the reference configurations correspond to squirmers which are relatively close to each other, and the pair moves away from $r \sim 1$. As it can be appreciated in fig. 3, type-B steady configurations show the largest displacements. Incidentally, in the limit $\alpha \to \alpha_c$ type-B.2 configurations degenerate into collinear ones (type A.2). Accordingly, these configurations exhibit a small region of stability which is not captured by the previous predictions at first order in the expansion in b_1 and b_2.

For perpendicular squirmers (type C), polarity determines their stable configurations even if they develop in regimes where apolar stresses are dominant ($\alpha < 1$). Hence, polarity stabilizes steady configurations controlled by active apolar stresses, as opposed to stable collinear configurations, where self-propulsion both promotes the

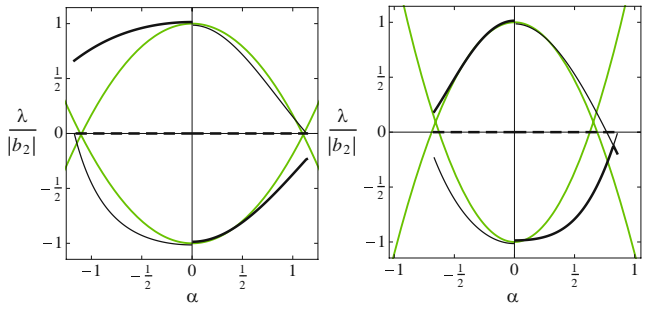

Fig. 6. (Colour online) Eigenvalues, λ_5 and λ_6, which determine the stability of parallel squirmers as a function of the relative apolar strength, α, for the same parameters introduced in fig. 2. The lines follow the same style as in fig. 5. a) Parallel (B.1) and b) antiparallel (B.2) orientations. The numerical results are plotted in black and the theoretical ones in green (light gray). The eigenvalues do not have imaginary components in these arrangements.

configurations and controls their stability. This qualitative change in the stability reflects in the functional dependence of the relevant eigenvalues,

$$\lambda_{5(6),1} = \frac{9}{32} b_1 \delta^2 (1 - \alpha) \pm i b_2 \sqrt{1 + \alpha - \alpha^2} \quad \text{(type C.1)},$$
$$\lambda_{5(6),1} = -\frac{9}{32} b_1 \delta^2 (1 + \alpha) \pm i b_2 \sqrt{1 - \alpha - \alpha^2} \quad \text{(type C.2)}. \tag{25}$$

The additional dependence of the characteristic time scales on the squirmers' separation, δ, reflects the fact that the configurations stability is determined by the coupling to the polar flow induced by the neigbour. The comparison with the numerical results, shown in fig. 7, captures the basic trends and the relevant time scales, but it is less accurate because the reference steady states derived in the appendix assume α small. This assumption, in particular, does not predict either that diverging configurations (type C.2) are always stable or that the stability change for extensile approaching configurations (type C.1). All the eigenvalues exhibit an imaginary component, indicating a frequency which scales like $1/\tau_2$. These oscillations evolve on shorter time scales than the typical relaxation time and should be observable.

6 Propagation of hydrodynamic interactions

The model analyzed accounts for particle inertia, as explicitly stated in eqs. (7) through the Reynolds number, Re. We have subsequently disregarded the squirmers' inertia and simplified the evolution equations correspondingly, eqs. (9), because for typical micro-organisms $Re \ll 1$. Even if inertia is negligible, for the typical distances between traps, a few times larger than the micro-organisms' size (*e.g.* $d \sim 10a$), in water the fluid flow induced by the squirmers takes a time $\tau_\nu = d^2/\nu \sim 0.1\,\mathrm{s}$ for opalina; for

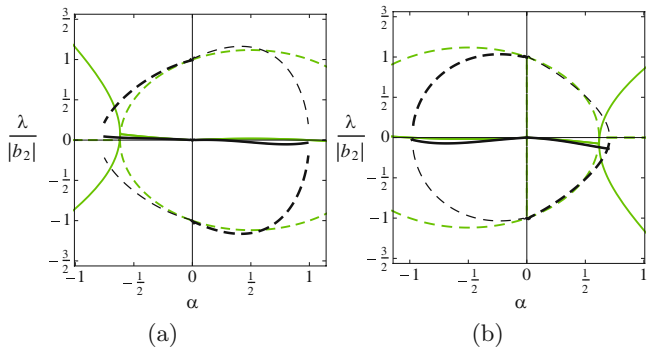

Fig. 7. (Colour online) Eigenvalues, λ_5 and λ_6, which determine the stability of perpendicular squirmers as a function of the relative apolar strength, α, for the same parameters introduced in fig. 2. The lines follow the same style as in fig. 5. a) Approaching (C.1) and b) diverging (C.2) orientations. Both real parts of the eigenvalues are equal.

smaller micro-organisms, *e.g.* of 10 μm in size, $\tau_\nu \sim 10^{-3}$ s. Therefore, the propagation of the hydrodynamic interactions between the two squirmers is not necessarily much smaller than the rest of relevant time scales, although in general the hierarchy $\tau_\nu < \tau_0 < \tau_1, \tau_2$ holds. Increasing the fluid viscosity, or reducing the trap stiffness will enlarge the separation of the diffusive time scale from the rest without affecting their relative ordering.

To address the effect of the hydrodynamic flow propagation on the steady configurations stability, we introduce a simple generalization and assume that one squirmer interacts at a given time, τ, with the flow induced by the neighbour at an earlier time $\tau - \tau_d$. Hence, we keep instantaneous interactions with a memory characterized by τ_d, which we will treat as a parameter related with τ_ν. The transient development of the flow field yields an interaction of a squirmer with a weighted velocity of the neighbour at earlier times characterized by a memory kernel. The proposed model corresponds to the simplest case where such a kernel reduces to a delta function located at an earlier time displaced by an amount τ_d. Since there is a time scale separation between the regime in which the flow develops and the time scales which control the stability of the steady configurations, disregarding the details of how the fluid flow develops will still capture the main effect that the fluid development has in the stability of the configurations the squirmers adopt in the traps.

For time delay equations, the eigenvalues which characterize the growth or decay of small perturbations around the steady configurations can be obtained assuming that they have an exponential dependence in time [38]. It is possible to derive the eigenvalue equations for the time-delayed dynamical system linearizing the system but separating the delayed and non-delayed contributions into different matrices. For the exponential dependence of the linearized variables we can arrive at a set of nonlinear equations for the eigenvalues [39] which can be solved numerically or perturbatively in powers of b_2 and assuming $\tau_d/\tau_0 < 1$. The time delay does not affect significantly the four fast decreasing modes which remain of order 1. Hence, the stability it is still determined by the two slow modes.

Analytic expressions can be derived if $\tau_d \kappa \lambda < 1$, satisfied if $\tau_d/\tau_0 < 1$. Furthermore, for simplicity's sake we consider that the delay is only relevant in the squirmers' orientations, consistent with the previous results which have shown the central role of the squirmers rotation on the stability of the steady configurations. Both for collinear comoving particles (type A.1) and diverging perpendicular squirmers (type C.2) the delay time affects those eigenvalues to second order in the expansion of eq. (19). As a result, the eigenvalues read

$$\begin{aligned}
\lambda_{5(6)} &= \pm b_2\sqrt{1-\alpha^2} - \frac{3}{4}b_1^2\delta - \tau_d\kappa b_2^2 \quad \text{(type A.1)},\\
\lambda_{5(6)} &= -\frac{9}{32}b_1\delta^2(1+\alpha) \pm ib_2\sqrt{1-\alpha-\alpha^2}\\
&\quad +\tau_d\kappa b_2^2 \quad \text{(type C.2)},
\end{aligned} \tag{26}$$

which show that time delay in the propagation of the hydrodynamic fields has an opposed effect in the two stable configurations. The stability of collinear stable configurations is not affected by the development of the velocity induced by the squirmers. For perpendicular diverging squirmers, increasing the delay time leads eventually to an unstable configuration, even in the range $\tau_d\kappa|b_2| \ll 1$. Hence, increasing the delay time relative to active temporal scales —increasing $\tau_d\kappa|b_2| \sim \tau_d/\tau_2$— can destabilize squirmers for values of α in which the configuration is stable for instantaneous coupling. The delay also affects the characteristic time scales in which relaxation develops for stable configurations and will have a significant effect when the delay becomes comparable to τ_2, a limit in which the assumed hierarchy between characteristic time scales breaks down. Thus, the delay in the development of the active flow patterns can have a significant impact in the configurations that pair of squirmers can develop.

Figure 8 shows the numerical results for the two relevant eigenvalues as a function of the delay time, and compare them with the theoretical predictions at small b_2, eqs. (26), for fixed b_2 and α. The figures quantify the relevance of delay in the values of the relaxation times and show the change in the stability of perpendicular configurations as the delay associated to the build-up of the hydrodynamic flow increases.

7 Discussion

We have analyzed the motion of pairs of squirmers confined by harmonic traps. Using Faxén theorem, we have derived their equations of motion and have described the relevant dimensionless parameters which control their collective behavior. In particular, for simple squirmers characterized by their self-propelling velocity through their polarity, B_1, and the active stress they generate around them in the absence of an intrinsic velocity, B_2, the ratio of these two amplitudes modulated by the amplitude of the hydrodynamic coupling characterized by the separation between the harmonic traps, controls the response of the system.

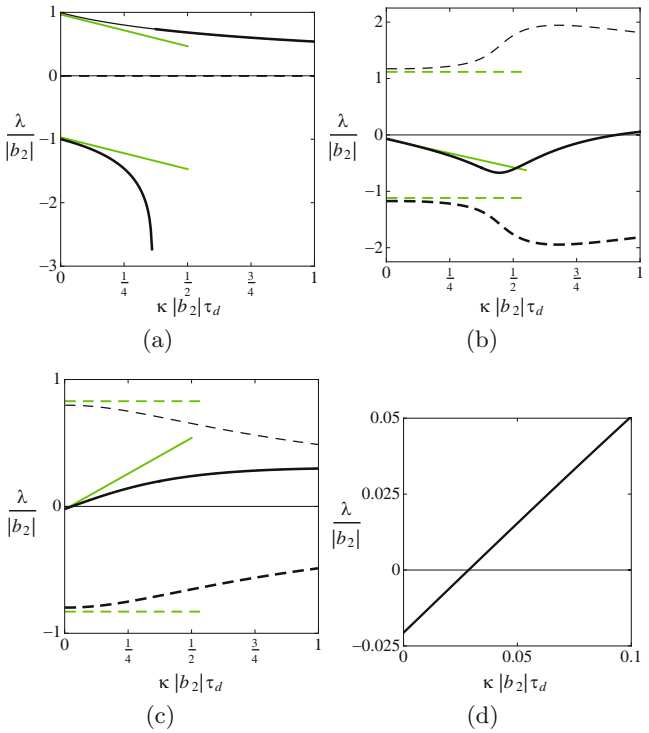

Fig. 8. (Colour online) Eigenvalues, λ_5 (black thin line) and λ_6 (black thick line), which determine the stability of collinear comoving squirmers (A.1) for (a) $\alpha = 0.25$ (unstable region) and (b) $\alpha = 1.5$ (stable region), and (c) the stability of diverging squirmers with perpendicular orientations (C.2) for $\alpha = 0.25$, as a function of the dimensionless delay parameter $\tau_d\kappa$ scaled with the dimensionless active time scale $1/|b_2|$. The rest of the parameters are the ones introduced in fig. 2. The green (light gray) line corresponds to the analytic predictions, valid for small $\tau_d\kappa|b_2|$. The real part of the eigenvalues are shown as solid lines and the imaginary contributions in dashed lines. (d) Zoom of the short-time behavior of the real part of the relevant eigenvalues for the perpendicular configuration displayed in (c) which shows the change in the stability.

We have characterized the steady configurations they reach as a result of the competition between their intrinsic self-propelling features, the confining harmonic potential induced by the trap and the flow generated by the neighbour. Three main configurations have been identified, which for completely apolar squirmers correspond to collinear (type A), parallel (type B) and perpendicular swimming (type C). Type-A configurations are stable for polar squirmers, while type-C ones become stable when the vorticity produced by the swimmers dominates.

The time scales which control the evolution towards or away from one of the steady configurations depend essentially on the squirmers self-propulsion. Stable configurations are controlled by a time scale which depends on the particle self-propulsion polarity $\tau_1 \sim d/B_1$ while unstable configurations evolve on time scales $\tau_2 \sim d/B_2\delta^2$ determined by the coupling through the active stresses. In some cases the squirmers will oscillate with a characteristic frequency which is always proportional to the active stresses, $1/\tau_2$.

For the typical sizes and velocities of micro-organisms, the time in which the induced velocity develops is usually smaller than or at most of the order of the time scale related to the trap stiffness, thus smaller than the time scale associated to squirmers' rotations. A simple model has captured the impact that such propagation has in the stability of the configurations that a pair of squirmers develop, and has identified its larger impact for perpendicular configurations, when the active stresses become the squirmers' dominant feature. Therefore, there exist regimes of squirmer motion where one must analyze the motion of the squirmers and the surrounding fluid flow on the same footing.

Although the analysis performed has neglected out-of-plane variations, as well as tumbling and noise, the results obtained and analyzed may be useful in experimental situations. We have shown that optical tweezers can be used to identify the effective active parameters which characterize the self-propulsion and the apolar stress generation of micro-organisms. The study has shown that the active velocity and stress produced by the squirmers determine the stable configurations as well as the relaxation times and frequency oscillations. The results obtained show how they can be used to measure the amplitude of the organism active velocity and generated stress. Since measurements can be carried out at different distances between the traps, and the self-propelling velocity of a squirmer can be measured by alternative means, there is room for precise measurements of the apolar active stresses. The use of cross correlation functions, as is done in other microrheology experiments [28], provides alternative procedures to get more accurate access to these relevant parameters.

The authors acknowledge Spanish MICINN (Project FIS2008-04386) and DURSI (SGR2009-634) for financial support.

Appendix A.

Analytic expressions for the steady configurations of the pair of trapped squirmers can be derived for small dimensionless squirmers' parameters b_1 and b_2. The results are obtained as an expansion in these parameters and explicit expressions are provided to first order.

Collinear squirmers (type A)

In terms of the variables introduced in eqs. (9), collinear squirmers moving parallel to each other (type A.1) arrive at a steady configuration at

$$\bar{\theta}_1 = 0, \qquad \bar{\theta}_2 = 0, \qquad \bar{\Psi} = \frac{\pi}{2},$$
$$\bar{r} \approx 1 + r_{\mathsf{A1}}, \qquad \bar{R}^r = \frac{b_1}{1+\hat{\delta}}, \qquad \tilde{R}^t = 0, \qquad \text{(A.1)}$$

with $r_{\mathsf{A1}} \equiv -\frac{b_2}{3}\frac{1}{1-\hat{\delta}}$, where we have introduced $\hat{\delta} \equiv \frac{3}{2}\delta$ and $b_1^0 \equiv \frac{4}{3}\frac{b_2\alpha}{\delta}$. We can already see that the polarity affects the displacement of the center of mass and the vorticity the displacement of the relative position (separation) between particles.

For collinear squirmers approaching (moving away from) each other we get instead

$$\begin{aligned} &\bar{\theta}_1 = 0\,(\pi), \qquad \bar{\theta}_2 = \pi\,(0), \qquad \bar{\Psi} = \frac{\pi}{2}\,, \\ &\bar{r} \approx 1 + r_{\mathsf{A3}}, \qquad \bar{R}^r = 0, \qquad \bar{R}^t = 0, \end{aligned} \tag{A.2}$$

where $r_{\mathsf{A3}} \equiv -2\frac{\frac{2}{3}b_2+(-)b_1}{1-\hat{\delta}}$.

For collinear swimming, squirmers only vary their relative positions; in this case the particles' orientations are fixed by the pair symmetry, and are hence exact. Also for symmetry reasons some of the displacements are exactly zero.

Parallel squirmers (type B)

Parallel squirmers (B.1) arrive at a position

$$\begin{aligned} &\cos\bar{\theta}_1 = \alpha(1-\hat{\delta}/2), \qquad \bar{\theta}_2 = \pi - \bar{\theta}_1, \qquad \bar{\Psi} = \frac{\pi}{2}\,, \\ &\bar{r} \approx 1 + r_{\mathsf{B1}}, \qquad \bar{R}^r = 0, \qquad \bar{R}^t = b_1\frac{\sqrt{1-\alpha^2(1-\hat{\delta})}}{1+\hat{\delta}/2}\,, \end{aligned} \tag{A.3}$$

with $r_{\mathsf{B1}} \equiv \frac{1}{1-\hat{\delta}}(\frac{2}{3}b_2 - 2b_1\alpha)$. The squirmer's orientations are given up to zeroth order in b_1 and b_2, $\bar{R}^r$ and $\bar{\Psi}$ in this configuration are exact.

Similarly, for antiparallel squirmers (B.2) we get

$$\begin{aligned} &\cos\bar{\theta}_1 = -\alpha(1+\hat{\delta}/2), \qquad \bar{\theta}_2 = \pi + \tilde{\theta}_1, \qquad \bar{r} \approx 1 + r_{\mathsf{B2}}\,, \\ &\bar{\Psi} = \frac{\pi}{2} - 2b_1\frac{\sqrt{1-\alpha^2(1+\hat{\delta})}}{1-\hat{\delta}/2}\,, \qquad \bar{R}^r = 0, \qquad \bar{R}^t = 0, \end{aligned} \tag{A.4}$$

where $r_{\mathsf{B2}} \equiv \frac{1}{1-\hat{\delta}}(\frac{2}{3}b_2 + 2b_1\alpha)$. Again with only zeroth order in squirmer's orientations and now with exact displacements $\bar{R}^r$ and $\bar{R}^t$.

Perpendicular squirmers (type C)

As there are no analytic results for the orientations in terms of b_1 and b_2, we need to make another expansion in powers of α. If we truncate this expansion at second order, which is a reasonable approximation as the perpendicular squirmers stationary solutions only exist for $\alpha < 1$, the results for the projections of the angles up to zeroth order in b_1 and b_2 are

C.1a(b)	$\sin\bar{\theta}_1 \approx \pm\hat{\delta}\alpha(1-\alpha)$,	$\cos\bar{\theta}_2 \approx \alpha(1-\hat{\delta}^2\alpha)$,
C.1c(d)	$\cos\bar{\theta}_1 \approx -\alpha(1-\hat{\delta}^2\alpha)$,	$\sin\bar{\theta}_2 \approx \pm\hat{\delta}\alpha(1-\alpha)$,
C.2a(b)	$\sin\bar{\theta}_1 \approx \mp\hat{\delta}\alpha(1+\alpha)$,	$\cos\bar{\theta}_2 \approx \alpha(1+\hat{\delta}^2\alpha)$,
C.2c(d)	$\cos\bar{\theta}_1 \approx -\alpha(1+\hat{\delta}^2\alpha)$,	$\sin\bar{\theta}_2 \approx \mp\hat{\delta}\alpha(1+\alpha)$.

The rest of the variables are also given not only up to first order in b_1 and b_2, as in the previous configurations, but also keeping the expansion in α

C.1a(b):

$$\begin{aligned} &\bar{r} \approx 1 + r_{\mathsf{C1}}, \\ &\bar{\Psi} \approx \frac{\pi}{2} + b_1\frac{1}{1-\hat{\delta}/2}(1 \mp \alpha\hat{\delta}/2 - 1), \\ &\bar{R}^r \approx -b_2\frac{1}{2(1+\hat{\delta})} + b_1\frac{1}{2(1+\hat{\delta})} + b_1\alpha\frac{1+\hat{\delta}/2}{1+\hat{\delta}}\,, \\ &\bar{R}^t \approx b_1\frac{1}{2(1+\hat{\delta}/2)}(1 \pm \alpha\hat{\delta}/2), \end{aligned} \tag{A.5}$$

with $r_{\mathsf{C1}} = -b_2\frac{1}{3(1-\hat{\delta})} - b_1\frac{1}{(1-\hat{\delta})} + b_1\alpha\frac{1-\hat{\delta}/2}{1-\hat{\delta}}$.

C.1c(d):

$$\begin{aligned} &\bar{r} \approx 1 + r_{\mathsf{C1}}, \\ &\bar{\Psi} \approx \frac{\pi}{2} - b_1\frac{1}{1-\hat{\delta}/2}(1 \mp \alpha\hat{\delta}/2), \\ &\bar{R}^r \approx b_2\frac{1}{2(1+\hat{\delta})} + b_1\frac{1}{2(1+\hat{\delta})} - b_1\alpha\frac{1+\hat{\delta}/2}{1+\hat{\delta}}\,, \\ &\bar{R}^t \approx b_1\frac{1}{2(1+\hat{\delta}/2)}(1 \pm \alpha\hat{\delta}/2). \end{aligned} \tag{A.6}$$

C.2a(b):

$$\begin{aligned} &\bar{r} \approx 1 + r_{\mathsf{C2}}, \\ &\bar{\Psi} \approx \frac{\pi}{2} + b_1\frac{1}{1-\hat{\delta}/2}(1 \mp \alpha\hat{\delta}/2), \\ &\bar{R}^r \approx -b_2\frac{1}{2(1+\hat{\delta})} - b_1\frac{1}{2(1+\hat{\delta})} + b_1\alpha\frac{1+\hat{\delta}/2}{1+\hat{\delta}}\,, \\ &\bar{R}^t \approx b_1\frac{1}{2(1+\hat{\delta}/2)}(1 \pm \alpha\hat{\delta}/2), \end{aligned} \tag{A.7}$$

with $r_{\mathsf{C2}} = -b_2\frac{1}{3(1-\hat{\delta})} + b_1\frac{1}{(1-\hat{\delta})} + b_1\alpha\frac{1-\hat{\delta}/2}{1-\hat{\delta}}$.

C.2c(d):

$$\begin{aligned} &\bar{r} \approx 1 + r_{\mathsf{C2}}, \\ &\bar{\Psi} \approx \frac{\pi}{2} - b_1\frac{1}{1-\hat{\delta}/2}(1 \pm \alpha\hat{\delta}/2), \\ &\bar{R}^r \approx b_2\frac{1}{2(1+\hat{\delta})} + b_1\frac{1}{2(1+\hat{\delta})} - b_1\alpha\frac{1+\hat{\delta}/2}{1+\hat{\delta}}\,, \\ &\bar{R}^t \approx b_1\frac{1}{2(1+\hat{\delta}/2)}(1 \mp \alpha\hat{\delta}/2). \end{aligned} \tag{A.8}$$

References

1. E.M. Purcell, Am. J. Phys. **45**, 3 (1977).
2. D. Bray, *Cell Movements: From Molecules to Motility* (Garland, New York, 2001).
3. M. Leoni, J. Kotar, B. Bassetti, P. Cicuta, M. Cosentino Lagomarsino, Soft Matter **5**, 472 (2009).
4. R. Dreyfus, J. Baudry, M.L. Roper, M. Fermigier, H.A. Stone, J. Bibette, Nature **437**, 862 (2005).
5. E. Lauga, Phys. Rev. Lett. **103**, 088101 (2009).
6. W.F. Paxton, K.C. Kistler, C.C. Olmeda, A. Sen, S.K.S. Angelo, Y. Cao, T.E. Mallouk, P.E. Lammert, V.H. Crespi, J. Am. Chem. Soc. **126**, 13424 (2004).
7. P. Tierno, R. Golestanian, I. Pagonabarraga, F. Sagués, Phys. Rev. Lett. **101**, 218304 (2009).
8. P. Tierno, O. Güell, F. Sagués, R. Golestanian, I. Pagonabarraga, Phys. Rev. E **81**, 011402 (2010).
9. G.P. Alexander, C.M. Pooley, J.M. Yeomans, Phys. Rev. E **78**, 045302 (2008).
10. P.T. Underhill, J.P. Hernández-Ortiz, M.D. Graham, Phys. Rev. Lett. **100**, 248101 (2008).
11. I. Llopis, I. Pagonabarraga, Europhys. Lett. **75**, 999 (2006).
12. I. Llopis, I. Pagonabarraga, Eur. J. Phys. E **26**, 103 (2008).
13. X. Wu, A. Libchaber, Phys. Rev. Lett. **84**, 3017 (2000).
14. Y. Hatwalne, S. Ramaswamy, M. Rao, R.A. Simha, Phys. Rev. Lett. **92**, 118101 (2004).
15. T.B. Liverpool, M.C. Marchetti, Phys. Rev. Lett. **97**, 268101 (2006).
16. D. Marenduzzo, E. Orlandini, Soft Matter **6**, 774 (2010).
17. D. Marenduzzo, E. Orlandini, M.E. Cates, J.M. Yeomans, Phys. Rev. E **76**, 031921 (2007).
18. S. Ramachandran, P.B.S. Kumar, I. Pagonabarraga, Eur. Phys. J. E **20**, 151 (2006).
19. G.I. Taylor, Proc. R. Soc. London, Ser. A **209**, 447 (1951).
20. G.I. Taylor, Proc. R. Soc. London, Ser. A **211**, 225 (1952).
21. A. Najafi, R. Golestanian, Phys. Rev. E **69**, 062901 (2004).
22. C.M. Pooley, G.P. Alexander, J.M. Yeomans, Phys. Rev. Lett. **99**, 228103 (2007).
23. M.J. Lighthill, Commun. Pure Appl. Math. **5**, 109 (1952).
24. J.R. Blake, J. Fluid Mech. **46**, 199 (1971).
25. T. Ishikawa, M.P. Simmonds, T.J. Pedley, J. Fluid Mech. **568**, 119 (2006).
26. I. Llopis, I. Pagonabarraga, J. Non-Newtonian Fluid Mech. **165**, 946 (2010).
27. T. Ishikawa, T.J. Pedley, Phys. Rev. Lett. **100**, 088103 (2008).
28. P. Bartlett, S.I. Henderson, S.J. Mitchell, Philos. Trans. R. Soc. London, Ser. A **359**, 883 (2001).
29. S. Chattopadhyay *et al.*, Proc. Natl. Acad. Sci. U.S.A. **103**, 13712 (2006).
30. A.D. Rowe *et al.*, J. Mod. Opt. **50**, 1539 (2003).
31. G.V. Soni, G. Ananthakrishna, G.V. Shivashankar, Appl. Phys. Lett. **85**, 2414 (2004).
32. K. Maeda, Y. Imae, J. Shioi, F. Oosawaj, J. Bacteriol. **127**, 1039 (1976).
33. G.W. Ordal, J. Bacteriol. **126**, 706 (1976).
34. J. Tailleur, M.E. Cates, EPL **86**, 60002 (2009).
35. S. Kim, S.J. Karrila, *Microhydrodynamics. Principles and Selected Applications* (Dover, Mineola, 1991).
36. R.M. Simmons, J.T. Finer, S. Chu, J.A. Spudich, Biol. J. **70**, 1813 (1996).
37. K.C. Neuman, A. Nagy, Nature **5**, 6 (2008).
38. Keqin Gu, V.L. Kharitonov, Jie Chen, *Stability of Time-Delay Systems* (Birkhäuser, Boston, 2003).
39. From the first-order dynamic system $\mathrm{d}\mathbf{x}/\mathrm{d}t = \mathbf{A}\cdot\mathbf{x}(t) + \mathbf{B}\cdot\mathbf{x}(t-\tau_d)$ we arrive at the characteristic equation $\mathrm{Det}(\mathbf{A} + e^{-\lambda\tau_d}\mathbf{B} - \lambda\mathbf{1}) = 0$ from which we can derive the eigenvalues λ.